Rapid Communications

Light irradiation induced brittle-to-ductile and ductile-to-brittle transition in inorganic semiconductors

Hongwei Wang,[1] Sergey I. Morozov,[2] William A. Goddard, III,[3,*] and Qi An[1,*]

[1]*Department of Chemical and Materials Engineering, University of Nevada-Reno, Reno, Nevada 89557, USA*
[2]*Department of Computer Simulation and Nanotechnology, South Ural State University, Chelyabinsk 454080, Russia*
[3]*Materials and Process Simulation Center, California Institute of Technology, Pasadena, California 91125, USA*

(Received 7 February 2019; revised manuscript received 2 April 2019; published 12 April 2019)

The intrinsic brittleness of inorganic semiconductors prevents them from extended engineering applications under extreme conditions of high temperature and pressure, making it essential to improve their ductility. Here, we applied the constrained density functional theory to examine the relationship between plastic deformation and photonic excitation in sphalerite ZnS and related II-IV semiconductors. We find that ZnS transforms from a dislocation dominated deformation mode in the ground state to a twin dominated deformation mode with bandgap electronic excitations, leading to brittle failure under light illumination. This agrees very well with recent mechanical experiments on single crystal ZnS. More interesting, we predict that the ZnTe and CdTe display the opposite mechanical behavior compared to ZnS, exhibiting ductility close to metallic level with bandgap illumination, but typical brittle failure in the dark state. Our results provide a general approach to design more shapeable and tougher semiconductor devices by controlling exposure to electronic excitation.

DOI: 10.1103/PhysRevB.99.161202

Inorganic semiconductors have attracted enormous attention because of their widespread applications in electronic devices, light-emitting diodes, thermoelectrics, and photovoltaic cells [1,2]. One of the main limitations in inorganic semiconductors is their brittle mechanical behavior. Fracture or yielding often occurs in these materials upon very small-scale strain induced by external stress [3–5]. Therefore, understanding, designing, and controlling of the mechanical properties of inorganic semiconductors are essential for their modern engineering applications. A very recent experimental study showed that sphalerite ZnS, a representative II-VI semiconductor, displays a brittle character under light irradiation [6], but, it becomes extraordinarily plastic when the deformation is performed in complete darkness. In addition, the brittle covalent compound GaAs also becomes more plastic [7] through the recombination of electron-hole pairs that are generated with the injected electrons by scanning electron microscopy. This suggested that the excited carriers play an opposite role in GaAs compared to ZnS. Thus, it is urgent to understand how the photon excited electron-hole pairs affect the dislocation properties in inorganic semiconductors, in order to provide a foundation for tuning the mechanical properties of semiconductors using bandgap light illumination.

It is well established that the formation and propagation of line defects (dislocations) [8,9], which is dependent on the strength of atomic binding forces [4,10,11], plays a crucial role in the mechanical properties of metals and semiconductors. An inorganic semiconductor α-Ag_2S with unusual metal-like ductility has recently been discovered experimentally [12] to undergo a large plastic deformation strain without fracture under mechanical stress. This is attributed to the relatively weak chemical bonding features of α-Ag_2S compared with other covalent semiconductors and ceramics. However, most inorganic semiconductors normally possess strong ionic or directional covalent bonds [4,5,13], which tend to resist their dislocation migration, leading to poor ductility. Hence, weakening the strength of atomic bonding may be an effective strategy to improve the ductility in ionic or covalent materials.

In our work, we employed the constrained density functional theory (CDFT) [14–20] to explore general stacking fault energy landscape of several II-VI ionic semiconductors for dislocation glide under light-irradiation condition, and explain our results by computing electrostatic energy of these ionic crystals [21]. We find that the modified energy landscape by electron-hole pairs has a significant effect on dislocations or twinning nucleation, leading to ductile behavior with dislocation nucleation or brittle behavior with twinning nucleation. Particularly, for ZnS we find that it tends to develop more deformation twinning under electron-hole excited states; while for other II-VI semiconductors, dislocation slip becomes the major deformation mechanism for plastic deformation. Twinning makes ZnS withstand smaller plastic strain and exhibit a brittle character; instead other II-VI semiconductors with more dislocation slip are likely to display a flexible character [22,23]. In the following sections, we discuss the detailed mechanism of light induced brittleness in ZnS crystal. Finally, some other ionic crystals are also predicted by us, which could become more ductility under light exposure conditions.

The dislocation properties in a crystal are closely related to the generalized stacking fault (GSF) energy (γ surface) from which one can derive dislocation core properties such as core width, Peierls stress using the Peierls-Nabarro model,

*Corresponding authors: qia@unr.edu; wag@caltech.edu

 ©2019 American Physical Society

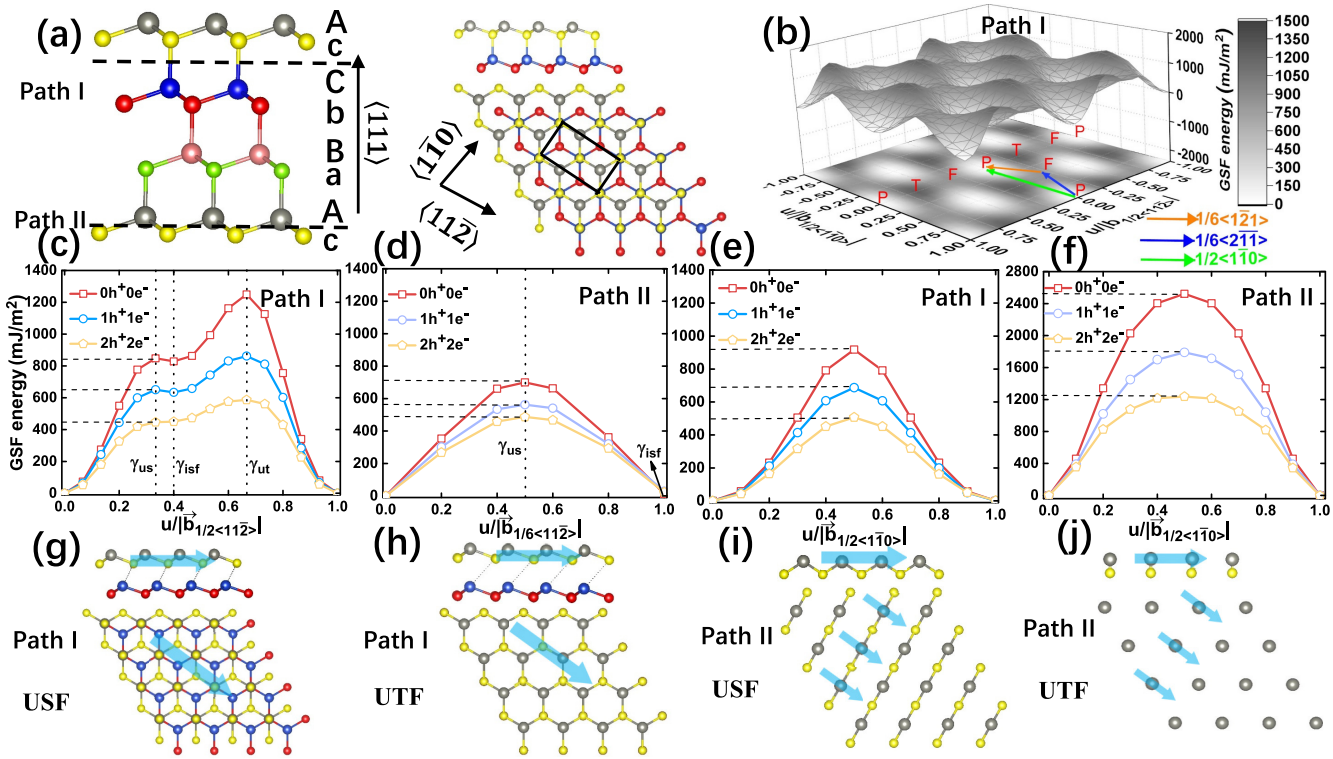

FIG. 1. (a) A schematic illustration showing the structure of sphalerite ZnS with the stacking sequence AaBbCc along the ⟨111⟩ direction and the top view of the {111} plane of ZnS based on the two normal vectors of ⟨11$\bar{2}$⟩ and ⟨1$\bar{1}$0⟩. A, B, C and a, b, c indicate Zn layers and S layers, respectively. The black rectangle denotes the normal Burgers vectors $1/2\langle 11\bar{2}\rangle a_0$ and $1/2\langle 1\bar{1}0\rangle a_0$. The dotted lines denote the two possible slip paths within the {111} plane of ZnS. Path I and path II indicate two plausible plastic deformation paths occurring between two widely spaced layers like Cc and two closely spaced layers such as Ac. (b) Three-dimensional GSF energy map of path I for the {111} plane of ZnS obtained by DFT calculation. P, F, and T represent perfect stacking, unstable stacking fault, and unstable twinning fault, respectively. (c), (d) GSF energy of path I (c) and path II (d) as a function of the displacement $u/|\vec{b}|$ along the ⟨11$\bar{2}$⟩ direction, where $\vec{b}$ is the length of the Burgers vector along the specific slip direction, and u denotes the magnitude of displacement. Here $0h^+0e^-$, $1h^+1e^-$ and $2h^+2e^-$ represent the results for the ground state, one electron-hole exited state, and two electron-hole excited state, respectively. γ_{us}, γ_{isf}, and γ_{ut} correspond to unstable stacking fault energy, intrinsic stacking fault energy, and unstable twin fault energy, respectively. (e), (f) GSF energy of path I (e) and path II (f) as a function of the displacement u/$|\vec{b}|$ along the ⟨1$\bar{1}$0⟩ direction. Schematic view of (g), (i) unstable stacking-fault structure, and (h), (j) unstable twinning-fault structure for ZnS. The blue arrows indicate the relative shift of top layer to bottom layer toward the ⟨11$\bar{2}$⟩ direction.

and the energy barrier for dislocation motion on a specific slip plane [24]. The major operative glide system for a sphalerite structure is well established to be $\{111\}\langle 1\bar{1}0\rangle$ [13,25–28]. As illustrated in Fig. 1(a), the glide plane of a dislocation in ZnS may lie

(1) either between a wide interlayer of stacking (path I) Aa, Bb, and Cc, or

(2) between narrow stacking layers of Ac, Cb, and Ba (path II) [25,29],

where A, B, C and a, b, c represent the atomic species of Zn and S, respectively. The shortest glide magnitude for these dislocations is described by the dislocation-displacement vector (or Burgers vector) of $\vec{b} = 1/2\langle 1\bar{1}0\rangle$, as shown in the γ surface [Fig. 1(b)]. Three nonequivalent saddle points exist on the entire γ surface: (1) the unstable stacking fault (USF) energy, γ_{us}, located at $1/6\langle 11\bar{2}\rangle a_0$; (2) the unstable twin fault (UST) energy, γ_{ut}, located at $1/3\langle 11\bar{2}\rangle a_0$; and (3) one located at $1/4\langle 1\bar{1}0\rangle a_0$. These three saddle points determine the energy barriers to slip along the ⟨11$\bar{2}$⟩ or ⟨1$\bar{1}$0⟩ directions. Particularly the γ_{us} and γ_{ut} play an important role for dislocation emission and microtwin formation [30–32]. They are marked as F and T on the projected energy contour map [the perfect stacking is labeled as P, Fig. 1(b)].

All-important energy configurations in the GSF landscape of sphalerite structure are along the ⟨11$\bar{2}$⟩ and ⟨1$\bar{1}$0⟩ directions. Therefore, we focus on the GSF curves along these two directions as a function of u/$|\vec{b}|$, as shown in Figs. 1(c)–1(f), where $|\vec{b}|$ is the length of a Burgers vector toward the specific slip direction, and u is the amount of slip displacement. The USF energy barrier in the ⟨1$\bar{1}$0⟩ direction is higher than that in the ⟨11$\bar{2}$⟩ direction for both path I and II, as shown in Figs. 1(c)–1(f). This indicates that it is energetically more favorable to partition the ⟨1$\bar{1}$0⟩ dislocation [green arrow in Fig. 1(b)] into two successive partials symmetry equivalent to the $1/6\langle 11\bar{2}\rangle a_0$ [blue and yellow arrows in Fig. 1(b)], which is in good agreement with previous work [22,25,33]. The displaced ZnS structures corresponding to USF and UST are illustrated in Figs. 1(g)–1(j) and the structure for perfect stacking is shown in Fig. 1(a). The figure shows that USF and UST originate from the relative shift between widely separated Zn-S layers for path I and narrowly spaced ones for path II, with the magnitudes of $1/6\langle 11\bar{2}\rangle a_0$ and $1/3\langle 11\bar{2}\rangle a_0$ for

USF and UST, respectively. The interlayer Zn-S ionic bonds are broken in both USF and UST configurations, resulting in a significantly increased energy barrier. Particularly, the seriously short Zn-S distance in the UST structure [Fig. 1(j)] accounts for the extremely large γ_{ut} of path II, which is almost three times that of path I. More details can be found in Fig. S1 of the supplementary material (SM) [34]. There is a shallow valley between γ_{us} and γ_{ut} for path I in the $\langle 11\bar{2}\rangle$ direction, denoted as intrinsic stacking fault energy γ_{isf}, as shown in Fig. 1(c). Only the GSF curve for partial slip $1/6\langle 11\bar{2}\rangle a_0$ is shown in Fig. 1(d) due to the very large γ_{ut} value for path II. The GSF curve of path II for the full Burgers vector $1/2\langle 11\bar{2}\rangle a_0$ is given in the Fig. S1 of the SM.

To illustrate how electron excitation affects the mechanical behavior of semiconductors, we compute the GSF energy curves of ZnS for electron-hole excited states, as depicted in Figs. 1(c)–1(f). The $0h^+0e^-$ represents the ground state without any electronic excitations, while $1h^+1e^-$ stands for the excited state with one electron located at the conduction band minimum (CBM) and one hole left at the valence band maximum (VBM). Similarly, $2h^+2e^-$ refers to the excited state with two electron-hole pairs. Figures 1(c)–1(f) indicates that the excited carriers cause a significant decrease in the GSF, leading to drastic changes in the mechanical properties. Particularly, the GSF energy surfaces for $1h^+1e^-$ and $2h^+2e^-$ states for path I are decreased by approximately 25 and 50% relative to that of $0h^+0e^-$ state, respectively. The total GSF of path II is also decreased by excited electron-hole pairs in the same trend, but less than path I. The value of γ_{us} for path II is lower than that of path I at the $0h^+0e^-$ state, suggesting that path II is more favorable at no excitation state, which agrees very well with previous experimental observations [25,29]. However, the electron-hole excitation causes the energy barrier of path I for dislocation slip to drop gradually below that of path II [see Figs. 1(c) and 1(d)], indicating an increased tendency for activating the dislocation slip along path I.

The above results suggest that electron-hole excitation by light irradiation should have a significant impact on the activation of dislocation slip in sphalerite ZnS, leading to changes of their mechanical behavior. The mechanical properties such as ductility and brittleness are determined by the unique deformation mechanisms. The ductility is dependent on the nucleation and propagation of dislocations, while brittle cleavage is initiated by crack formation [35]. Dislocation slip and deformation twinning are two primary mechanisms for plastic deformation and energy dissipation in many face-centered-cubic materials [30,35]. It has been well established that twin boundaries are more effective to strengthen the materials by blocking the dislocation motion compared to conventional grain boundaries, leading to a more brittle character [23]. On the contrary, the dislocation with the low slip barrier tends to make materials more ductile. Previous work found that twinning and slip generated via dislocations occur on the same set of slip systems, exhibiting a strongly competitive relationship [35]. Tadmor and Bernstein defined the twinnability to describe this competition [30], which plays an important role in determining ductile (dislocation slip) versus brittle (twinning) behavior. The essential parameters for evaluating the twinnability are γ_{us}, γ_{ut}, and γ_{isf}, which can be obtained from the GSF landscape. The derived expression for the twinnability is dependent on the ratios of γ_{isf}/γ_{us} and γ_{us}/γ_{ut} [30,36].

As shown in Fig. 1(c), the ratio γ_{isf}/γ_{us} for path I is close to unity in ionic sphalerite compounds, therefore the criterion for twinning tendency can be approximated as $\sqrt{\gamma_{us}/\gamma_{ut}}$ [35]. In addition, the twinnability for path II should be much smaller compared with path I, due to the extremely large γ_{ut} of path II. Hence, we only discuss the twinnability for path I instead of path II in the present work. A summary of the values for γ_{us}, γ_{ut}, and twinnability τ of path I are given in Table SI. The twinnability for ZnS increases with additional electronic excitation. Although the increased twinnability for ZnS is small, the fraction of twin-related texture in real systems is extremely sensitive to its change. For example, the difference of twinnability for Ag and Al metal is about 0.1, but the difference twin-related texture is almost 90% [36]. Therefore, under light-irradiation conditions, ZnS is expected to develop more deformation twinning through path I, leading to the brittle performance. On the other hand, path II with small twinnability is the energy favorable slip plane in darkness, which tends to create dislocation slip, leading to the ductile character. Our prediction agrees very well with previous experiments on ZnS [6] indicating that the switch of the deformation mechanism from dislocation to twinning leads to the change from ductile deformation at dark environment to brittle failure under light irradiation.

In order to understand why electronic excitation affects the GSF landscape in ZnS, we analyzed the bonding and charge features. Figure 2(a) displays the contour of electron localization function (ELF) [37] in the {111} plane, which can measure the extent of electron pair localization. The ELF values are between 0 and 1, representing electron pairs that are perfect localized (ELF = 1) or complete delocalized (ELF = 0), respectively. The electrons tend to localize around S atoms, indicating ionic bonding character in the ZnS crystal. Figures 2(b)–2(c) describe the charge density difference between the $0h^+0e^-$ and $1h^+1e^-$ states for the USF structures of path I and II. The charge density difference is obtained by subtracting the charge density of $1h^+1e^-$ state from that of $0h^+0e^-$ state. The blue isosurface on the S site and the red isosurface on the Zn site describe losing electron at S^{2-} anion and capturing electron at Zn^{2+} cation at the slip plane, respectively. Figures 2(d)–2(e) show the planar average difference charge density along the $\langle 111\rangle$ direction (the average value for charge density difference on the {111} plane) between the $0h^+0e^-$ and $1h^+1e^-$ states for the USF structures of path I and II. These analyses indicate that the charge density increases at the Zn site and decreases at the S site at each slip plane as dislocation slip occurs. The direct consequence of charge transfer from S^{2-} anion to Zn^{2+} cation would lead to neutral atoms, reducing their electrostatic interactions at the slip plane. In addition, the VBM and CBM contributed partial charge densities to the S and Zn ions at the slip plane (see Fig. S2 in the SM). This indicates that there will be donor states at the S sites and acceptor states at the Zn sites, consistent with the charge density analysis. The same charge density analysis for the UST structure is displayed in Fig. S3 of the SM. Likewise, the electrons follow the same

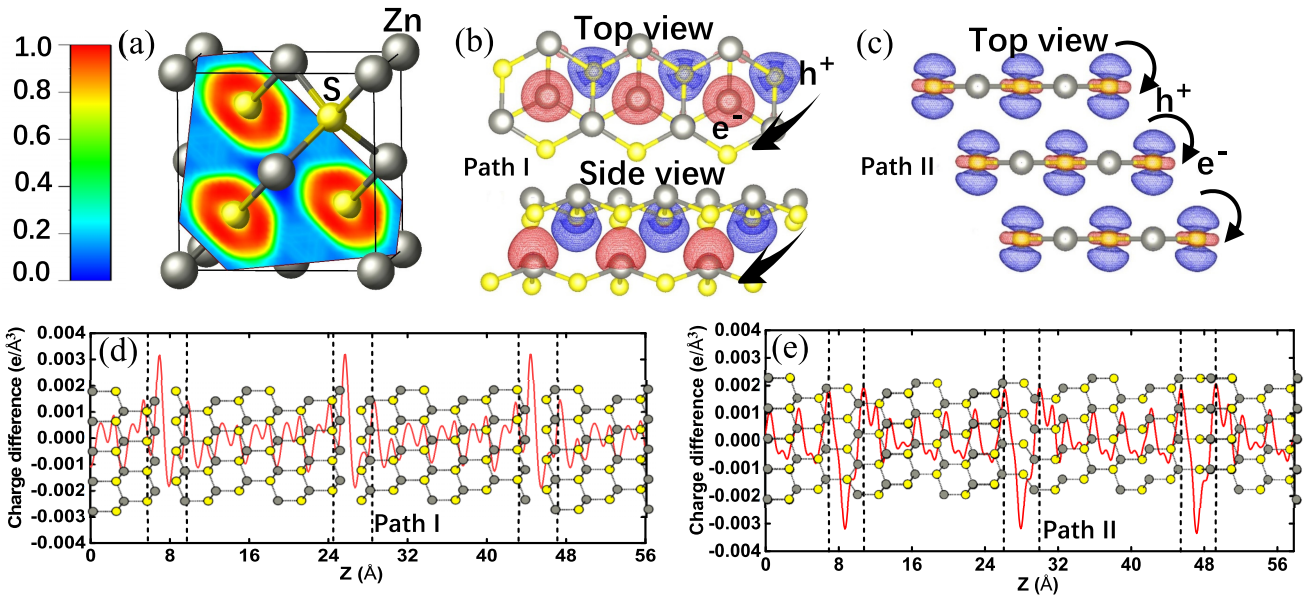

FIG. 2. (a) Electron localization function maps in the {111} plane of the ground state. (b), (c) Charge density difference between the ground state and one electron-hole excited state for the unstable stacking-fault structure of (b) path I and (c) path II. The blue and red color isosurfaces denote losing and capturing electrons. (d), (e) Planar average charge density difference [(d) path I, (e) path II] between the ground state and one electron-hole excited state for the unstable stacking-fault structure along the ⟨111⟩ direction.

transfer process with electron-hole excitation, as that in USF structure.

For path II, the decreased Zn-S bonds due to dislocation slip would lift the acceptor states at the Zn sites to a high energy level, far above the CBM (see Fig. S2 in the SM). Consequently, the excited electrons fail to be captured by Zn cations at the slip plane. As shown in Figs. 2(c) and 2(e), the charge density obviously decreases at S sites, but is almost unchanged on Zn sites. As discussed above, the reason for the GSF energy landscape to be reduced by the exited electron-hole pairs can be understood as follows. The dislocation motion in ionic crystal breaks the ionic bonds between the slip planes, providing additional charges to the dislocation. The charged dislocations in the crystal generate static fields, which act on the dislocations to inhibit further movements [38]. When light-irradiation induces electron-hole pairs, the charged dislocations are discharged. This can weaken the static fields to make the motion of charged dislocations energetically more favorable. Moreover, the reason for the weaker dependence of γ surface on electron-hole excitation in path II is because the exited electrons are not trapped at the Zn sites, which cannot effectively reduce the charge of Zn cations, as well as the related electrostatic interactions at the slip planes.

Besides the ZnS compound, we have also investigated other similar II-VI semiconductors ZnSe, ZnTe, and CdTe [6,13,39–41]. The ELF analysis for these systems, shown in Fig. S4 of the SM, indicates that all of these sphalerite materials can be classified as ionic crystals. Therefore, we can apply the same physical framework of ZnS to explain the activation of the dislocation motion in ZnSe, ZnTe, and CdTe. The GSF curves along the $\langle 11\bar{2}\rangle$ direction for ZnSe, ZnTe, and CdTe are shown in Fig. 3 and Fig. S5 of the SM. Since the dislocation motion in sphalerite structures occurs along the $\langle 11\bar{2}\rangle$ direction, the γ surface along the $\langle 1\bar{1}0\rangle$ direction is not considered. Similar to ZnS, the γ surface are dramatically reduced in all of these sphalerite systems with the electronic excitation, and their energy barriers at the same electronic state follow a ranking of ZnS > ZnSe > ZnTe > CdTe. The variation of the γ surface of ZnSe and ZnTe with electron-hole concentration is quite similar to that of ZnS. The dislocation glide prefers to occur along path II at the $0h^+0e^-$ ground state, whereas path I becomes more energy favorable for dislocation motion for increased electronic excitation. However, Path I for CdTe has a lower activation energy for dislocation motion than Path II for all electronic states, which we attribute to the increased Cd-Te repulsive forces by Cd^{2+} with large ionic radius in the closed stacking Path II. It is worth noting that the γ_{us} of ZnTe and CdTe at the $2h^+2e^-$ state are about 200 mJ/m^2 for path I, which is close to that of metallic systems such as Mg and Al [30], and are expected to display extraordinary ductility under strong light illumination. The bonding force in ionic crystals originates primarily from the electrostatic interaction between ions, which is sensitive to the dielectric constant. As a result, the larger dielectric constants of ZnTe and CdTe (listed in Table SI) reduce the electrostatic interaction, accounting for their low energy barrier for dislocation motion. The reason for the larger dielectric constants in ZnTe and CdTe is their smaller bandgaps, as shown in Table SI. The high-frequency dielectric constant is inversely proportional to the square of bandgap, as proposed in previous theoretical studies [42].

Using the same framework, we next analyze the twinnability for these II-IV semiconductors. The twinnability for ZnSe is slightly increased with the electronic excitation. For ZnTe and CdTe, the twinnability decreases and is unchanged, respectively, with increased exited electron-hole pairs. In contrast to ZnS, we find that CdTe and ZnTe should become

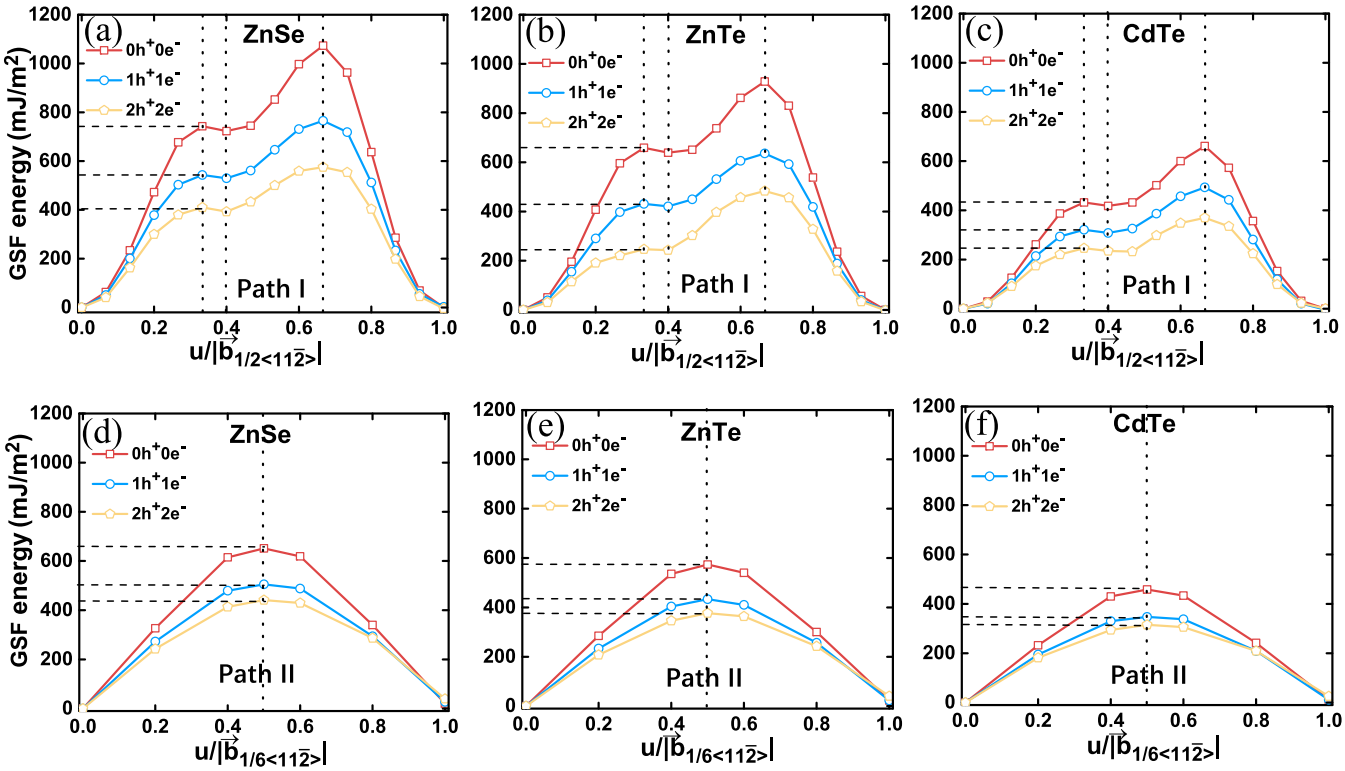

FIG. 3. GSF energies for both path I and path II associated with the displacement along the $\langle 11\bar{2}\rangle$ direction for (a) ZnSe, (b) ZnTe, and (c) CdTe.

more ductile with light illumination, which results from their significantly reduced energy barrier for dislocation slip as well as their unchanged or even decreased twinnability.

Finally, we utilize the Madelung model [21] to calculate the electrostatic energy resulting from long-range ionic coulomb interactions to illustrate the mechanism for electronic excitation induced mechanical behaviors of ZnS and related materials. The variation of the Madelung energy per unit area with $u/|\vec{b}|$ for path I is plotted in Fig. S6 of the SM. Interestingly, the Madelung energy decreases much faster for the UST structure than for the USF structure for electronic excitation in ZnS. This reduces the difference between γ_{us} and γ_{ut}, accounting for the increased twinnability. The strong ionic coulomb forces in ZnS give rise to the large difference between γ_{us} and γ_{ut}. When the electrostatic interactions are weakened by electronic excitation, the difference between γ_{us} and γ_{ut} and related twinnability are significantly reduced as well. Similarly, ZnSe possessing more moderate coulomb forces shows a slightly increased twinnability. Furthermore, the electrostatic interactions in ZnTe and CdTe are weaker compared with ZnS, thus their twinnability displays a different performance.

In summary, we used CDFT to determine how the bandgap electronic excitation affects mechanical behaviors of several sphalerite ionic crystals. The ionic charges carried by dislocations are reduced by electron-hole pairs created by light irradiation, which can effectively reduce the electrostatic interactions and modify the energy landscape for dislocation motion. This significantly affects the twinnability, which measures the tendency for whether the plastic deformation develops through dislocation slip or through deformation twinning. Under bandgap light illumination, the ionic compounds with stronger electrostatic interactions tend to increase the twinnability leading to a brittle character, in excellent agreement with recent experiments [6]. In contrast, for systems with increased covalent character, the weaker ionic coulomb forces result in improved ductility under bandgap electronic irradiation. Thus, we predict that ZnTe and ZnSe materials will possess metal-like ductility under strong photoexcitation. It is worth mentioning that the photon induced carrier concentration in our theoretical calculation is about $10^{21}/\text{cm}^3$ order of magnitude, which may need to be realized experimentally through the strong, hard light.

This work was supported by the National Science Foundation (NSF) (CMMI-1727428).

The authors declare that they have no competing financial interests.

[1] P. Y. Yu and M. Cardona, *Fundamentals of Semiconductors: Physics and Materials Properties* (Springer, Berlin, 1996).

[2] M. Cardona and Y. Y. Peter, *Fundamentals of Semiconductors* (Springer, Berlin, 2005).

[3] Y. Umeno and M. Černý, Phys. Rev. B **77**, 100101(R) (2008).

[4] S. Ogata, Y. Umeno, and M. Kohyama, Model. Simul. Mater. Sci. Eng. **17**, 013001 (2008).

[5] S. Ogata, J. Li, N. Hirosaki, Y. Shibutani, and S. Yip, Phys. Rev. B **70**, 104104 (2004).

[6] Y. Oshima, A. Nakamura, and K. Matsunaga, Science **360**, 772 (2018).

[7] P. G. Callahan, B. B. Haidet, D. Jung, G. G. Seward, and K. Mukherjee, Phys. Rev. Mater. **2**, 081601 (2018).

[8] P. M. Anderson, J. P. Hirth, and J. Lothe, *Theory of Dislocations* (Cambridge University Press, Cambridge, 2017).

[9] D. Hull and D. J. Bacon, *Introduction to Dislocations* (Butterworth-Heinemann, Oxford, 2001).

[10] N. De Leon, X.-X. Yu, H. Yu, C. R. Weinberger, and G. B. Thompson, Phys. Rev. Lett. **114**, 165502 (2015).

[11] S. Ogata, J. Li, and S. Yip, Science **298**, 807 (2002).

[12] X. Shi, H. Chen, F. Hao, R. Liu, T. Wang, P. Qiu, U. Burkhardt, Y. Grin, and L. Chen, Nat. Mater. **17**, 421 (2018).

[13] R. Whitworth, Adv. Phys. **24**, 203 (1975).

[14] B. Kaduk, T. Kowalczyk, and T. Van Voorhis, Chem. Rev. **112**, 321 (2011).

[15] M. Melander, E. O. Jónsson, J. J. Mortensen, T. Vegge, and J. M. García Lastra, J. Chem. Theory Comput. **12**, 5367 (2016).

[16] D. Kidd, A. S. Umar, and K. Varga, Phys. Rev. B **98**, 075108 (2018).

[17] J. P. Perdew, K. Burke, and M. Ernzerhof, Phys. Rev. Lett. **77**, 3865 (1996).

[18] G. Kresse and J. Hafner, Phys. Rev. B **47**, 558 (1993).

[19] G. Kresse and D. Joubert, Phys. Rev. B **59**, 1758 (1999).

[20] P. E. Blöchl, Phys. Rev. B **50**, 17953 (1994).

[21] K. Momma and F. Izumi, J. Appl. Crystallogr. **44**, 1272 (2011).

[22] G. Vanderschaeve, in *Solid State Phenomena* (Trans Tech Publications, Zurich, 1998), p. 145.

[23] Y. Zhu, X. Liao, and X. Wu, Prog. Mater Sci. **57**, 1 (2012).

[24] G. Lu, N. Kioussis, V. V. Bulatov, and E. Kaxiras, Phys. Rev. B **62**, 3099 (2000).

[25] C. Speake, P. Smith, T. Lomer, and R. Whitworth, Philos. Mag. A **38**, 603 (1978).

[26] M. P. Kulakov and S. Z. Shmurak, phys. stat. sol. (a) **59**, 147 (1980).

[27] L. Huang and S. Wang, J. Appl. Phys. **124**, 175702 (2018).

[28] M. Ukita, R. Nagahara, Y. Oshima, A. Nakamura, T. Yokoi, and K. Matsunaga, Mater. Trans. **60**, 99 (2019).

[29] V. Petrenko and R. Whitworth, Philos. Mag. A **41**, 681 (1980).

[30] E. Tadmor and N. Bernstein, J. Mech. Phys. Solids **52**, 2507 (2004).

[31] B. Li, M. Sui, and S. Mao, J. Mater. Sci. Technol. **27**, 97 (2011).

[32] A. Frøseth, H. Van Swygenhoven, and P. Derlet, Acta Mater. **52**, 2259 (2004).

[33] A. Nakamura, M. Ukita, N. Shimoda, Y. Furushima, K. Toyoura, and K. Matsunaga, Philos. Mag. **97**, 1281 (2017).

[34] See Supplemental Material at http://link.aps.org/supplemental/10.1103/PhysRevB.99.161202 for (i) computational details, (ii) the partial charge densities for VBM and CBM orbitals, (iii) charge transfer process in ZnS under electronic excitations for UST structure of path I, (iv) computed parameters of the γ surface, bandgaps, and dielectric constants for sphalerite ionic crystals, (v) bonding features in sphalerite crystals, and (vi) the response of electrostatic energy to the dislocation displacement in sphalerite ionic crystals.

[35] E. B. Tadmor and S. Hai, J. Mech. Phys. Solids **51**, 765 (2003).

[36] N. Bernstein and E. B. Tadmor, Phys. Rev. B **69**, 094116 (2004).

[37] A. Savin, R. Nesper, S. Wengert, and T. F. Fässler, Angew. Chem. Int. Ed. Engl. **36**, 1808 (1997).

[38] J. Gilman, J. Appl. Phys. **44**, 982 (1973).

[39] M. Al-Kuhaili, A. Kayani, S. Durrani, I. Bakhtiari, and M. Haider, ACS Appl. Mater. Interfaces **5**, 5366 (2013).

[40] D. Chadi, Phys. Rev. Lett. **72**, 534 (1994).

[41] G. Fonthal, L. Tirado-Mejıa, J. Marın-Hurtado, H. Ariza-Calderon, and J. Mendoza-Alvarez, J. Phys. Chem. Solids **61**, 579 (2000).

[42] S. Wemple and M. Di Domenico, Jr., Phys. Rev. B **3**, 1338 (1971).